1 Towards a dark matter experiment

C. Amsler, V. Boccone, W. Creus, L. Scotto Lavina, P. Otyugova, C. Regenfus, and J. Rochet

(ArDM and DARWIN Collaborations)

We are constructing at CERN a 1 ton liquid argon detector (ArDM) to detect both charge and luminescence produced by recoil nuclei, following a WIMP interaction. WIMPs (Weak Interacting Massive Particles) are prime candidates for the dark matter in the universe.

Charged particles lead to ionization and excitation of argon atoms, forming excimers with the lowest singlet and the triplet excited states decaying by VUV photon emission in a narrow band around 128 nm. The singlet and the triplet states have different decay times, respectively $\tau_1 \simeq 5$ ns and $\tau_2 \simeq 1.6$ μs in liquid (1). However, impurities such as water, air and CO_2, can absorb the VUV light and reduce τ_2 (2). The population ratio singlet/triplet depends on ionization density. For minimum ionizing projectiles, such as electrons and photons, the ratio is ≈ 0.3, while for alpha particles and nuclear recoils one finds a ratio of ≈ 4 (1). Hence nuclear recoils from WIMPs populate mostly the fast decaying singlet state. In addition, the ionization yield is much lower for nuclear than for minimum ionizing particles. This is due to quick recombination which decreases the charge and enhances the luminescence. The higher ratio of light to charge production for nuclear recoils and the higher population of the fast decaying state can both be used to reduce background in WIMP searches.

The ArDM experiment consists of a 1 t liquid argon (LAr) detector to search for WIMPs interacting elastically with argon nuclei. A sketch illustrating the measurement principle is shown in Figures 1.1 and 1.2. The apparatus collects signals from scintillation and ionization independently. The ionization charges drift towards the gas phase in an electric field of

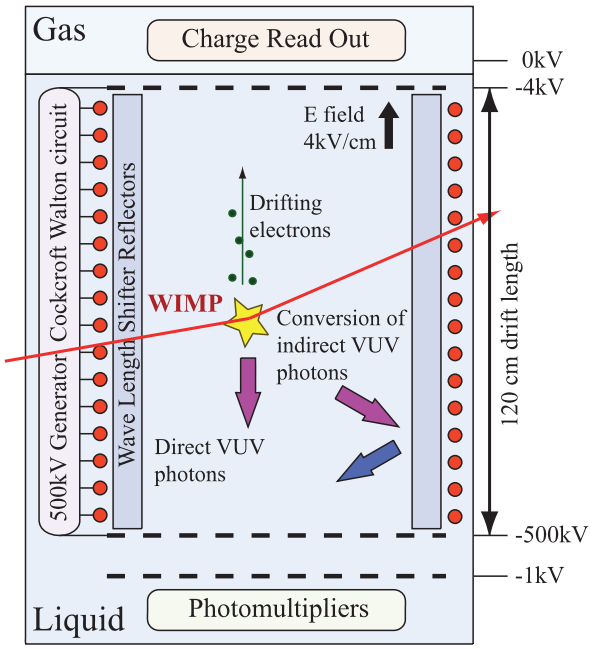

Figure 1.1:
Conceptual layout of the ArDM experiment.

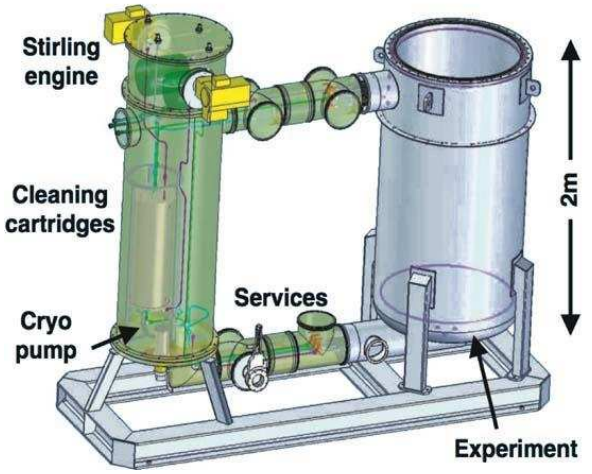

Figure 1.2:
3D sketch of the ArDM cryogenic setup with LAr cleaning circuit and main dewar.

4 kV/cm supplied by a Greinacher (Cockroft-Walton) chain with 210 stages. The charge is extracted from the liquid into the gas phase by a high electric field between two extraction grids (below and above the liquid surface). A large area electron multiplier (LEM) is used to amplify the charge. The field shaping rings are covered on their inner sides with reflectors to shift the 128 nm fluorescence light into the visible range and to increase the light collection efficiency (3). Fourteen photomultipliers (PMT) are located below the HV cathode (–500 kV). The fiducial mass of the detector is estimated to be about 850 kg. The LAr recirculation and purification system (based on a CuO cartridge), provides the purity for drift distances of up to 120 cm. A 3D sketch of the detector is shown in Fig. 1.2.

The detector is currently installed on the surface in building 182 at CERN and our group has developed the light

readout system. The ArDM detector was filled for the first time with 1 ton of LAr in May 2009 (4). Several important parameters such as cryogenic operation at high LAr purity over weeks, stable and flawless operation of the light readout system, high scintillation light yield, and detection of events down to energies of the order of tens of keV could be verified.

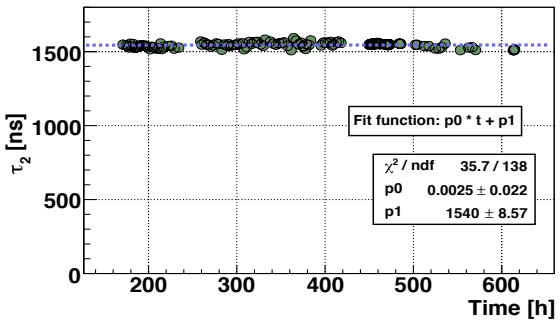

Figure 1.3: Monitoring of the LAr purity in ArDM from the slow luminescence component τ_2 during 600h of operation.

The test was performed with a partial light readout assembly consisting of 7 (instead of 14) Hamamatsu R5912-MOD PMTs with Pt-underlays, no electric field and no charge readout. The PMT glass was coated with a thin layer of a transparent TPB-paraloid compound to increase the collection efficiency for VUV light. The side reflectors were made of 15 Tetratex foils (120×25 cm^2), coated with Tetraphenyl butadiene (TPB) wavelength shifters (WLS) of optimum thickness (5), using a custom made evaporator. The apparatus was filled with LAr with the side reflectors fully immersed and kept full for about 3 weeks, while various measurements with radioactive sources were performed.

The monitoring of the LAr purity was performed by measuring the decay time of the slow component of the light signal (τ_2) (2). The purity was found to be constant (Fig. 1.3), around $\tau_2 \simeq 1.5$ μs, in agreement with expectations (1). Figure 1.4 shows the fluctuations of the PMT calibration constants as a function of time.

To study the detector response to photons we used a ^{22}Na source (E$_\gamma$=511 keV and 1274 keV) and a ^{137}Cs source (E$_\gamma$=661 keV). For ^{137}Cs the data were obtained with the LAr detector in self-trigger mode, while for ^{22}Na the detector was in coincidence with an external NaI scintillator. The response spectra in

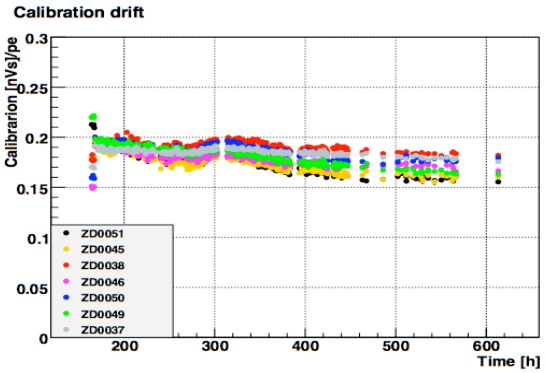

Figure 1.4: Fluctuation of the PMT calibration constants as a function of time.

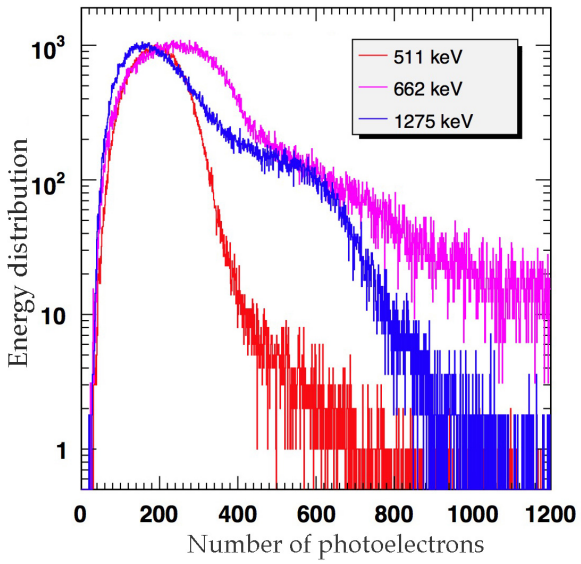

Figure 1.5: Energy spectra for ^{137}Cs and ^{22}Na.

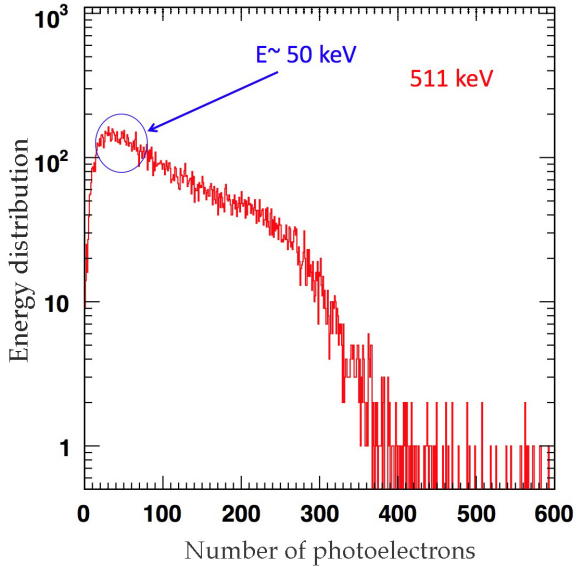

Figure 1.6: Energy distribution for 511 keV γs.

Fig. 1.5. The shapes of the distributions can be reproduced and fitted assuming multiple Compton scattering in the detector (7). The light yield is estimated to be $\sim$0.5 photoelectrons/keV for electrons with the 7 PMTs assembly. Furthermore, by triggering on the total energy deposited by two of the three γs (511 and 1275 keV) we could select the signal from the second 511 keV γ in LAr. Figure 1.6 shows that a lower threshold of 50 keV for electrons can be reached already with 7 PMTs.

Even small neutron fluxes around 1 MeV are potentially dangerous, since the neutron-argon cross section is some 18 orders of magnitude larger than for WIMPs. It is therefore essential to investigate the response of the dark matter detector to neutrons as a function of recoil energy. We first studied the detector response to neutrons from an Am-Be source producing 3×10^4 1/s neutrons in the 1 – 10 MeV range. Data were taken for different positions of the source. Figure 1.7 shows the ratio CR between the integrated pulse height of the prompt light ($<$ 50 ns) and that of the total light, as a function of integrated pulse height. These data were taken with the source located on the upper flange of the detector. As expected, neutrons leading to the nuclear recoil band (N.R.) mainly populate the fast decaying singlet state. Figure ?? (left) also shows the contributions from γs leading to Compton electrons (E.R. band). The corresponding decay time distributions for the two bands are shown in Fig. 1.8, fitted with exponentials convoluted with Gaussians.

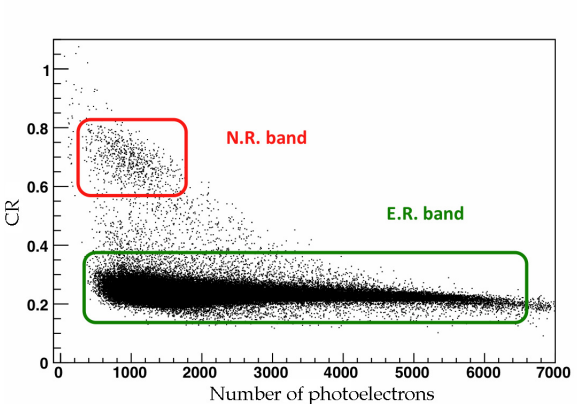

Figure 1.7:
Ratio CR of fast to total amplitude for the Am-Be-source on the top flange of the ArDM detector. The upper box shows nuclear recoils (N.R.), the lower box electron recoils (E.R.).

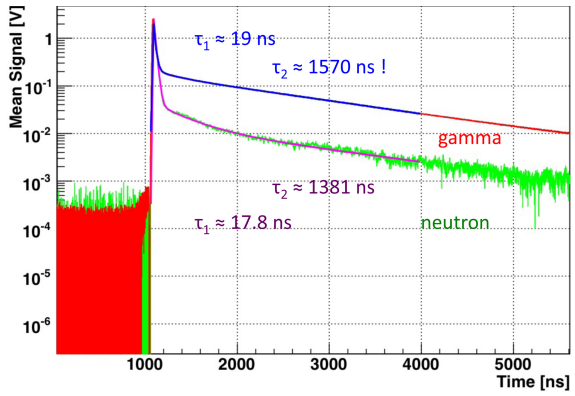

Figure 1.8: Decay time distributions corresponding to the two regions indicated in Fig. 1.7 with the fast and the slow components.

The ArDM detector was upgraded in summer 2009 to the final 14 PMTs. The deposition of WLS on the PMT windows was performed using a fast evaporation technique at the thin film laboratory of CERN. A photograph of the array under UV illumination before installation in the ArDM detector is shown in Figs. 1.9.

In autumn 2009 measurements were started in gaseous argon (GAr, Ar60 at room temperature and 1.1 bar pressure) using a movable ^{241}Am source (5.5 MeV αs) to obtain an estimate for the light yield with the fully equipped light readout. We collected data immediately after GAr filling to evaluate the maximum purity reached with the new turbopump system, then gathered more data as a function of time to observe the purity degradation. The best vacuum level reached before filling was 10^{-5} mbar, for which the measured slow component of the excimer-state decay τ_2 was found to be 3.04±0.04 μs, in accord with known values in gas at atmospheric pressure (2). Figure 1.10 shows for each PMT with a measurement of the mean life τ_2 of the slow component, the degradation of argon purity as a function of time.

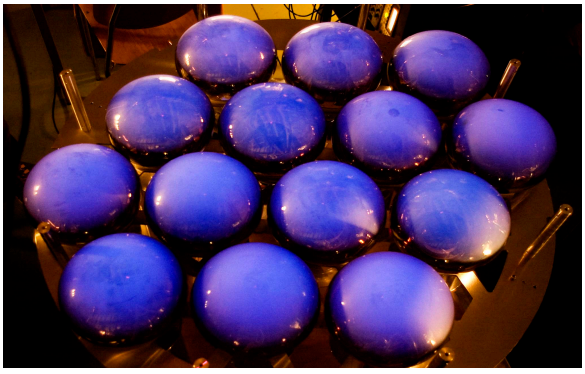

Figure 1.9: The 14 cryogenic PMTs coated with WLS, ready to be installed at the bottom of the ArDM apparatus, illuminated with UV light.

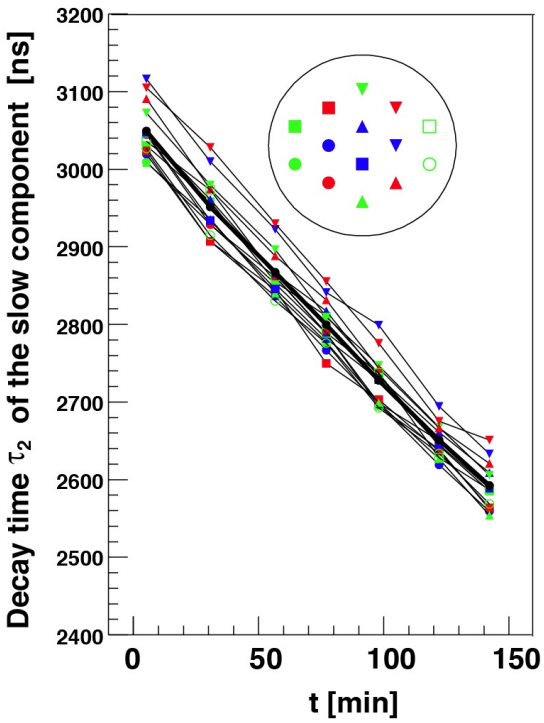

Figure 1.10: Measurement of the slow component of the luminescence in gaseous argon as a function of time (see text), for various source positions in the detector and for different PMTs (inset).

We have also contributed to the online data acquisition system and to the offline software. We developed, starting from the previous existing software, and a new analysis framework to satisfy basic needs, namely easy and fast access to the data, a modular package to include the forthcoming charge readout, which can also incorporate Monte Carlo

data. The package was used to analyze the late 2009 data. For example, the signal offset was previously evaluated for each event by assessing the average value of the pedestal (before event trigger time), and by rejecting events for which the width of the pedestal distribution was exceeding a preset value. In the new approach a peak finding algorithm is applied instead to the pedestal trace, searching for anomalies such as PMT dark counts, background photons, and pile-up events. Also, PMTs near the detector edges collect less light due to geometrical inefficiencies. This makes the selection of e.g. αs less inefficient from single PMTs and more prone to background. Instead, the new framework applies all cuts on the total light collected from the 14 PMTs.

As already mentioned, neutrons with energies around 1 MeV or less will contribute to the background in WIMP searches. On the other hand, radioactive neutron sources can be used to study the luminescence yield from nuclear recoils in noble liquids (Fig. ?? above). Heavily ionizing particles such as recoiling nuclei generate significantly less light than electrons (for equal energy deposits). The quenching factor and its dependence on energy are poorly known for LAr and LXe, but lies in the range 0.15– 0.30 (8). We intend to measure the quenching factor as a function of recoil energy down to 10 keV by studying neutron-argon and neutron-xenon scattering with monoenergetic neutrons. Furthermore, the probability for multiple neutron interactions is large (while WIMPs interact only once). This can be studied with monoenergetic neutrons in a large cell (and in ArDM). This R&D work will benefit to both ArDM and the design of a next-generation noble liquid dark matter facility in Europe (DARWIN), which was recently funded by ASPERA, and to which we participate (together with the group of Prof. L. Baudis).

We have therefore purchased a neutron source from NSD-Fusion GmbH. The source delivers monoenergetic 2.45 MeV neutrons (up to 10^7 s^{-1}) from the reaction dd $\rightarrow$He^{3}n. The fusion generator, designed and optimised in collaboration with the maufacturer, was delivered at the end of 2009. The generator is based on a high voltage plasma discharge (30 - 120 kV, 1 - 15 mA). The gas pressure is controlled by heating getter disks which store the deuterium on their surfaces. Due to the excellent efficiency of the shielding the radiation dose remains far below the limit of 2.5 μSv/h at maximum fluence, and we are authorized to operate the generator at CERN without further shielding, but within a closed fence with safety and radiation interlock against X-rays, γs and neutrons (Figs. 1.11 and 1.12).

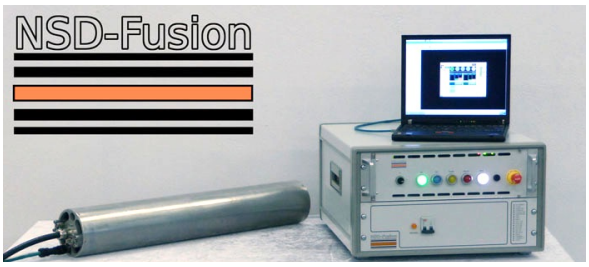

Figure 1.11: Components of the neutron generator (fusion chamber, HV power supply and controller).

Figure 1.12: Installation in the laboratory showing the 1600 kg cylindrical shielding (grey) made of water extended polyester (WEP) mixed with a boron absorber (Colemanite, $CaB_3O_4(OH)_3{\cdot}H_2O$).

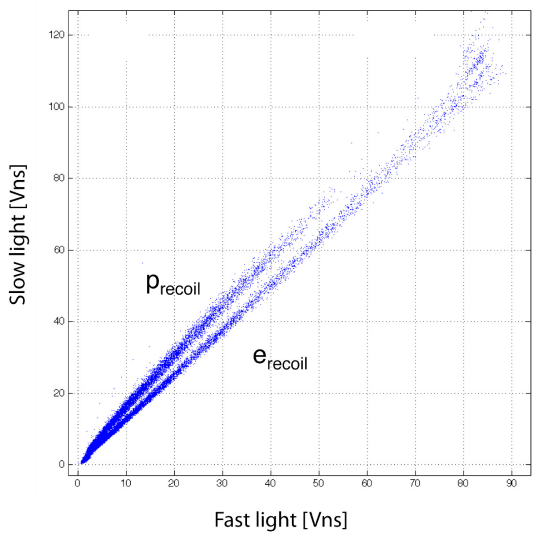

Figure 1.13: Proton and electron separation in liquid scintillator from the Am-Be source. Plotted is the distribution of integrated pulse height vs. integrated pulse height within the first 15 ns.

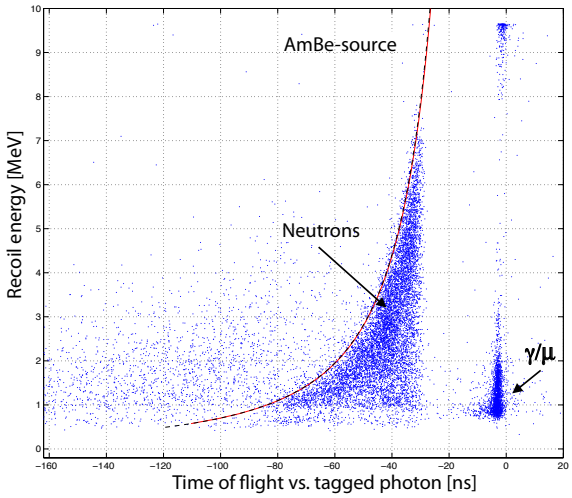

Figure 1.14: Recoil proton energy vs. time-of-flight. The red line shows the expected boundary. The accumulation on the far right is due to γs and cosmic muons.

The generator is routinely running in our laboratory and we are currently completing the system with a collimator, mechanical parts to hold the test chamber, and neutron detector components for the scattering experiment.

Three liquid EJ301 scintillator cells (diameters 2, 3 and 5″) were purchased from SCIONIX. They are suitable for fast neutrons ($>$ 50 keV) and give information on the neutron energy, the recoiling proton being absorbed in the cell. However, calibration is required due to the non-linearity of light output vs. proton energy. Typically half of the 2.45 MeV neutrons scatter on the carbon component and are not detected. Protons and electrons lead to different pulse shapes in the scintillator (Fig. 1.13). A precise timing ($<$ 1ns) can be achieved to select neutron energies by time-of-flight. We have performed measurements on the 3″ detector with a 370 MBq Am-Be source located at a distance of about 1m. The source produced $3{\cdot}10^4$ n/s from the αBe reaction in the energy range 1 – 10 MeV. The neutron energy could be measured by time-of-flight by triggering on a 4.4 MeV γ (from $^{13}C^*$ decays) emitted in coincidence, and compared with the measured proton recoil energy (Fig. 1.14).

In the setup sketched in Fig. 1.15 neutrons from the dd-source are scattered in the 3″ scintillation counter and detected under the angle θ by the 5″ counter. Figure 1.16 shows the proton recoil spectra for neutrons in the 3″ target counter which would be uniform (due to the isotropic scattering in the c.m.s.) in the absence of multiple scattering, scattering on carbon and for infinite energy resolution. Figure 1.17 shows the sum of energy deposits in both counters (for θ = 45°) which should ide-

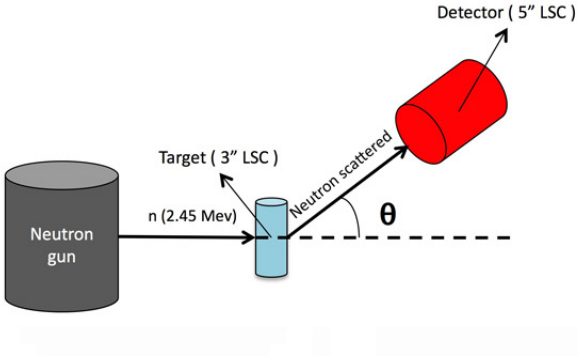

Figure 1.15: Sketch of the scattering experiment.

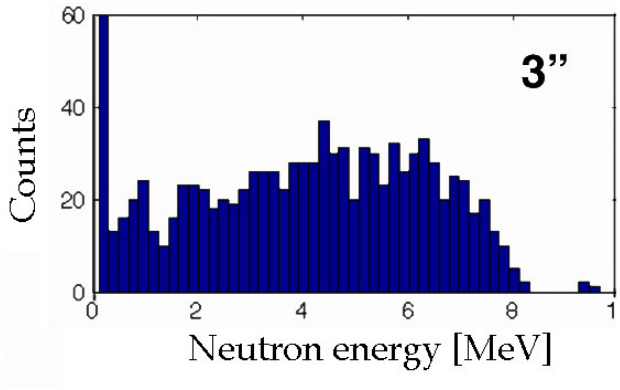

Figure 1.16: Proton recoil energy distribution in the 3” target counter.

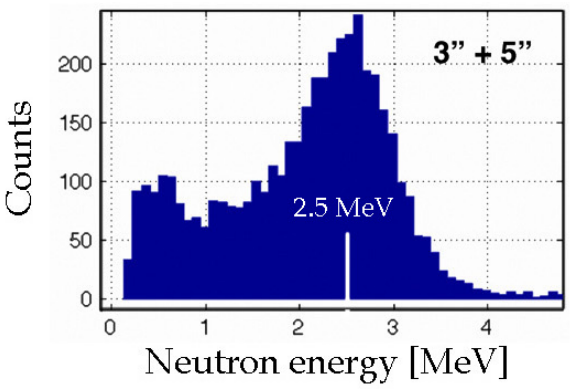

Figure 1.17: Sum of the energy deposits in the 3” and 5” counters.

ally be equal to the initial neutron energy. Indeed the distribution peaks around the expected incident energy of 2.5 MeV. The low energy enhancement is due to energy losses in the collimator.

R&D work for subdetector components is now being finalized and the results for the light readout efficiency are quite encouraging. The next run of the LAr detector equipped with 14 PMTs and a simple anode plane for the charge readout is planned for July 2010. This run should bring the experiment close to the point when physics operation could start. Pending are the construction and installation of the LEMs for the charge readout, and the implementation of a cryocooler and improved liquid recirculation system (H_2O filter). These items are in the hands of the ETHZ group. Upon completion, the detector will be moved to an underground location, probably the Canfranc underground laboratory in the Pyrenees.

[1] A. Hitachi *et al.*, Phys. Rev. **B27** (1983) 5279

[2] C. Amsler *et al.*, Journal of Instrumentation **3** (2008) P02001

[3] V. Boccone *et al.*, Journal of Instrumentation **4** (2009) P06001

[4] C. Amsler, Proc. 2009 Conf on HEP, Krakow (2009), PoS(EPS-HEP 2009)110;
P. Otyugova, Proc. 5th Patras Workshop on Axions, WIMPs and WISPs (2009);
C. Regenfus, Proc. TAUP 09 Conf., Rome, prep. arXiv:0912.2962v1 [phys.ins-det] (2009)

[5] H. Cabrera, Master Thesis, Universität Zürich (2007)

[6] C. Amsler *et al.*, Journal of Instrumentation **3** (2008) P02001

[7] V. Boccone, PhD thesis, Universität Zürich, in preparation

[8] D. M. Mei *et al.* Astropart. Phys. **30** (2008) 12